Coherence-assisted superradiant laser with hertz-level linewidth and 10^{-10}-W power

Guohui Dong [1,2] Yao Yao [3] Peng Zhang,[4,5,*] and Dazhi Xu [6,5,†]

[1]*School of Physics and Electronic Engineering, Sichuan Normal University, Chengdu 610068, China*
[2]*Graduate School of China Academy of Engineering Physics, Beijing 100084, China*
[3]*Microsystem and Terahertz Research Center, China Academy of Engineering Physics, Chengdu 610200, China*
[4]*Department of Physics, Renmin University of China, Beijing 100872, China*
[5]*Beijing Computational Science Research Center, Beijing 100084, China*
[6]*Center for Quantum Technology Research and Key Laboratory of Advanced Optoelectronic Quantum Architecture and Measurements (MOE), School of Physics, Beijing Institute of Technology, Beijing 100081, China*

(Received 31 January 2023; accepted 7 June 2023; published 26 June 2023)

The superradiant laser, based on the clock transition between the electric ground state $^1S_0$ and the metastable state $^3P_0$ of fermionic alkaline-earth-metal-like atoms, has been proposed to be a new promising light source with linewidth of the order of millihertz. However, due to the small $^1S_0$ to $^3P_0$ transition strength, the steady-state power in that system is relatively low (approximately 10^{-12} W). In this work we propose an alternative superradiant laser scheme based on a Raman-transition-induced coupling between the $^3P_0$ and $^3P_1$ states in bosonic alkaline-earth-metal-like atoms and achieve a laser with narrow linewidth (less than approximately $2\pi \times 1$ Hz) and high power (greater than approximately 10^{-10} W, approximately 10^3 photons in steady state) at a small pumping cost (less than approximately $2\pi \times 10$ kHz). The Raman beams play two significant roles in our scheme. First, the coherence between the dark and bright states induced by the Raman beams produces a new local minimum in the pumping-linewidth curve with pumping rate lower than $2\pi \times 10$ kHz, which is beneficial for continuous output. Second, the Raman beams mix the long-lived $^3P_0$ state into the lasing state and thus make the laser linewidth tunable. Our work greatly improves the output performance of the superradiant laser system with coherence induced by Raman transitions and may offer a firm foundation for its practical use in the future.

DOI: 10.1103/PhysRevA.107.063709

I. INTRODUCTION

Nowadays, the narrow-linewidth laser finds its importance in both fundamental scientific interest and practical applications, such as determining physical constants, gravitational wave detection, and global positioning systems [1–5]. The traditional frequency stability method uses a rigid Fabry-Pérot cavity as a reference, which is fundamentally limited by thermal fluctuations of the cavity length [6–10]. In the past decade, instead of further reduction of thermal noise of the reference cavity, the superradiant laser that utilizes the atomic transition with a long lifetime, such as the $^1S_0$ to $^3P_0$ clock transition of fermionic alkaline-earth-metal atoms, was proposed and has attracted much attention. Unlike the traditional laser, the superradiant laser works in the bad-cavity regime where the cavity loss is several orders of magnitude larger than the atomic decay [11–18]. Thus the cavity mode can be eliminated adiabatically in this regime, leading to a strong atom-atom correlation (a collective spin) [13,19–21], and the coherence of the superradiant laser is solely stored in the atoms. The most attractive feature of the superradiant laser is that its linewidth can be smaller than the corresponding atomic decay rate with frequency robust against cavity length fluctuation [12,15].

However, in previous superradiant laser systems, it was hard to achieve a laser with both a narrow linewidth and high power at the same time. For instance, due to the long-lifetime nature of the $^3P_0$ state in fermionic alkaline-earth-metal atoms, the weak coupling of the $^1S_0$ to $^3P_0$ transition to the cavity field prevents the system from outputting a high power, while the scheme with bosonic alkaline-earth-metal atoms possesses a stronger coupling to the cavity field but a much broader laser linewidth of about $2\pi \times 1$ kHz, achieved with a pumping rate of several tens of kilohertz [15]. In fact, theoretical studies have also shown that the laser linewidth in the scheme with bosonic alkaline-earth-metal atoms can be reduced to the hertz level when the pumping strength is increased to several megahertz [17]. Considering that the superradiant laser has been experimentally demonstrated based on the $^1S_0$ to $^3P_0$ transition in ^{87}Sr [14] and the $^1S_0$ to $^3P_1$ transition in ^{88}Sr [15], we expect to propose a scheme with both advantages of these two systems, i.e., narrow linewidth and appreciable power.

To this end, we propose to couple the $^3P_0$ state to the $^3P_1$ state in the bosonic alkaline-earth-metal atom (e.g., ^{88}Sr) by Raman transitions. The $^3P_0$ state has an extremely long lifetime which can effectively suppress the spontaneous decay rate of the lasing state. Meanwhile, the laser power can get significantly increased compared to the system with fermionic alkaline-earth-metal atoms, since the $^1S_0$ to $^3P_1$ transition

*pengzhang@ruc.edu.cn
†dzxu@bit.edu.cn

assists in the lasing process. The idea of this proposal stems from our previous work [22] where we produced a Raman-transition-assisted ultranarrow transmission spectrum based on magnetically induced optical transparency [23].

The second-order mean-field calculation shows that our proposed scheme can realize a superradiant laser with a $2\pi \times 1$ Hz level linewidth and 10^{-10}-W level power (approximately 10^3 photons in steady state) at a small pumping rate of $2\pi \times 10$ kHz. Interestingly, in the pumping-linewidth curve, apart from the local minimum point that also appears in other superradiant laser systems, a new local minimum emerges in our scheme with a small pumping rate. The above narrow-linewidth, high-power, and low-pumping output laser is created by this new minimum. The feature of this low-pumping rate can inhibit the heating effect in the lasing process and thus is very beneficial for continuous output. Further analyses and calculations illustrate that the double-minimum character in linewidth originates from the coherence between the dark and bright states induced by the Raman transitions. This is the most attractive feature of our scheme over those without Raman beams.

The remainder of this paper is organized as follows. We introduce our setup and the calculation methods in Secs. II and III, respectively. In Sec. IV, by taking the ^{88}Sr atomic ensemble as the working medium, we illustrate the power, linewidth, and pulling coefficients of the superradiant laser in our proposal. In Sec. V we investigate the double-minimum behavior of the linewidth in the frame with respect to the dark and bright states. Section VI provides a summary and discussion of our results. Details of the calculations are given in Appendixes A and B.

II. MODEL

A. System setup

In our system, as shown in Figs. 1(a) and 1(b), an ensemble of N cold bosonic alkaline-earth-metal-like atoms are trapped in an optical cavity with the axis along the y direction. The quantization axis of the atomic angular momentum is along the z direction and $J_z = m_J\hbar$ (we set $\hbar = 1$ hereinafter) is the projection on the z axis. The x-polarized cavity mode couples with the lasing transition between the electronic $^1S_0$ state $|g\rangle$ and the $^3P_1$ state $|x\rangle$, which is defined as

$$|x\rangle \equiv \frac{1}{\sqrt{2}}(|^3P_1, m_J = -1\rangle - |^3P_1, m_J = +1\rangle). \tag{1}$$

Two Raman beams α and β are employed to effectively couple the $^3P_1$ state to the long-lived $^3P_0$ state. The y-polarized beam α couples the state $|x\rangle$ to the $^3S_1$ ($m_J = 0$) state $|S\rangle$ and the z-polarized beam β couples $|S\rangle$ to the $^3P_0$ state $|P\rangle$.

B. Lasing process

Before the detailed calculation, it is necessary to present a rough and qualitative description of how the laser is generated in our scheme. The pumping process incoherently transfers the atoms from the ground state $|g\rangle$ to the excited state $|S\rangle$. (One possible pumping scheme includes three pumping beams: The first beam pumps the atom from $^1S_0$ to $^3P_1$, the second one from $^3P_1$ to $^3S_1$ probably with a large detuning, and the last one from $^3S_1$ to $5s6p\,^3P_1$, which then decays to $^3S_1$. The second and third beams are two-photon resonant with the atomic transition from $^3P_1$ to $5s6p\,^3P_1$.)

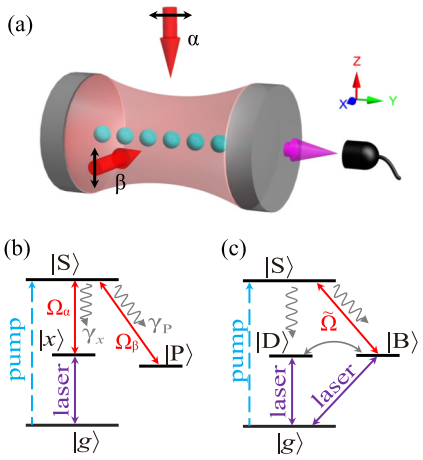

FIG. 1. (a) N bosonic alkaline-earth-metal-like atoms are trapped in an optical cavity. Two Raman beams α and β polarized in the y and z directions, respectively, are injected into the cavity. (b) Schematic diagram of the four-level lasing system. The atoms are incoherently pumped to the $^3S_1$ state $|S\rangle$ and then transit to the $^3P_1$ state $|x\rangle$ or the $^3P_0$ state $|P\rangle$ via spontaneous decay or Raman-induced coupling. The atoms in $|x\rangle$ further transit to the $^1S_0$ state $|g\rangle$ and emit laser photons into the cavity mode. (c) Schematic diagram of our scheme in the basis with dark state $|D\rangle$ and bright state $|B\rangle$. The atoms in state $|S\rangle$ can transit to $|D\rangle$ via only spontaneous decay and to $|B\rangle$ via both spontaneous decay and the Raman transition. The atoms in both $|B\rangle$ and $|D\rangle$ can emit laser photons.

Some of the atoms in the $^3S_1$ state will fall to the state $|x\rangle$ or $|P\rangle$ via either the spontaneous decay or Raman-beam-induced coherent transitions. As the $^3P_0$ to $^1S_0$ transition of bosonic alkaline-earth-metal atoms is electric dipole forbidden (e.g., ^{24}Mg, ^{40}Ca, and ^{88}Sr) [24], it does not couple with the cavity mode. Hence, when the population inversion is established between $|x\rangle$ and $|g\rangle$ and the stimulated emission overwhelms the photon loss, the laser polarized in the x direction will be generated.

Although the $^1S_0$ to $^3P_0$ transition does not directly couple with the laser mode, the Raman-induced coherence between the $^3P_0$ and $^3P_1$ states plays a crucial role in reducing the linewidth, which is similar to our previous work on the ultranarrow transmitted spectrum [22]. An appropriate way to investigate this coherence is revisiting the above lasing scheme utilizing the dark ($|D\rangle$) and bright ($|B\rangle$) states corresponding to the Raman coupling, which are defined as

$$|D\rangle \equiv (\Omega_\beta|x\rangle - \Omega_\alpha|P\rangle)/\tilde{\Omega}, \tag{2}$$

$$|B\rangle \equiv (\Omega_\alpha|x\rangle + \Omega_\beta|P\rangle)/\tilde{\Omega}. \tag{3}$$

Here $\Omega_{\alpha\,(\beta)}$ is the Rabi frequency corresponding to the Raman beam α (β) and $\tilde{\Omega} \equiv \sqrt{|\Omega_\alpha|^2 + |\Omega_\beta|^2}$ is the Raman strength.

Figure 1(c) shows the same lasing scheme as Fig. 1(b) but uses the basis of $|D\rangle$ and $|B\rangle$. We can see that the state $|S\rangle$ couples with only the bright state $|B\rangle$ through the Raman beams with effective coupling intensity $\tilde{\Omega}$. Thus, besides the spontaneous decay, the pumped state $|S\rangle$ can also transit to

the state $|B\rangle$ via the Raman transition. In contrast, the state $|S\rangle$ transits to the state $|D\rangle$ only through the spontaneous decay. As both states $|D\rangle$ and $|B\rangle$ have the $|x\rangle$ component, the lasing mode coherently couples with both the $|D\rangle$-$|g\rangle$ and $|B\rangle$-$|g\rangle$ transitions. It is remarkable that there exists an incoherent coupling between $|D\rangle$ and $|B\rangle$, which comes from the spontaneous decay of the state $|S\rangle$.[1] We will show the explicit calculation of the laser properties using the bare basis $|x\rangle$ and $|P\rangle$ in Sec. III and Appendix A and discuss the influence of coherence between the dark and bright lasing transitions on the laser linewidth in Sec. V.

III. MODEL AND METHODS

In this section we use the second-order mean-field master equation to calculate the laser power, frequency, and linewidth in our scheme.

A. Hamiltonian and master equation

The Hamiltonian, including the N atoms, the quantized cavity field, and the classical Raman beams, is given by

$$\begin{aligned}\hat{H} = {} & \omega_c \hat{a}^\dagger \hat{a} + \sum_{j=1}^{N} \left(\omega_0 \hat{\sigma}_{xx}^{(j)} + \omega_S \hat{\sigma}_{SS}^{(j)} + \omega_P \hat{\sigma}_{PP}^{(j)}\right) \\ & + \sum_{j=1}^{N} \left(\frac{\Omega_c}{2} \hat{a}^\dagger \hat{\sigma}_{gx}^{(j)} + \frac{\Omega_\alpha}{2} \hat{\sigma}_{Sx}^{(j)} e^{-i\omega_\alpha t} \right. \\ & \left. + \frac{\Omega_\beta}{2} \hat{\sigma}_{\mathrm{SP}}^{(j)} e^{-i\omega_\beta t} + \mathrm{H.c.} \right), \end{aligned} \tag{4}$$

where $\hat{a}$ ($\hat{a}^\dagger$) is the annihilation (creation) operator of the cavity mode with angular frequency ω_c and

$$\hat{\sigma}_{\mu\nu}^{(j)} \equiv |\mu\rangle^{(j)}\langle\nu| \quad (\mu, \nu = g, x, S, P) \tag{5}$$

is the electronic state transition operator for the jth atom. We choose the energy of the electronic ground state $|g\rangle$ to be zero and then the frequencies of the states $|x\rangle$, $|S\rangle$, and $|P\rangle$ are ω_0, ω_S, and ω_P, respectively. The angular frequencies of the Raman beams α and β are ω_α and ω_β, respectively. Here Ω_c is the Rabi frequency of the atom-cavity coupling and $\Omega_{\alpha\,(\beta)}$ is that of the Raman-induced coupling between the state $|S\rangle$ and $|x\rangle$ ($|P\rangle$). We assume that all the atoms homogeneously interact with the optical cavity and the Raman beams. Without loss of generality, we choose all the Rabi frequencies as real.

In the rotated frame, the above Hamiltonian (4) can be simplified as

$$\begin{aligned}\hat{H}_I = {} & \delta_c \hat{a}^\dagger \hat{a} + \sum_{j=1}^{N} \left[\delta_\alpha \hat{\sigma}_{SS}^{(j)} + (\delta_\alpha - \delta_\beta)\hat{\sigma}_{PP}^{(j)}\right] \\ & + \sum_{j=1}^{N} \left(\frac{\Omega_c}{2} \hat{a}^\dagger \hat{\sigma}_{gx}^{(j)} + \frac{\Omega_\alpha}{2} \hat{\sigma}_{Sx}^{(j)} + \frac{\Omega_\beta}{2} \hat{\sigma}_{\mathrm{SP}}^{(j)} + \mathrm{H.c.} \right), \end{aligned} \tag{6}$$

[1]One can find this coupling by writing the master equation (10) in the basis of $|D\rangle$ and $|B\rangle$.

where the detunings are defined as

$$\delta_c \equiv \omega_c - \omega_0, \tag{7}$$

$$\delta_\alpha \equiv \omega_S - \omega_0 - \omega_\alpha, \tag{8}$$

$$\delta_\beta \equiv \omega_S - \omega_P - \omega_\beta. \tag{9}$$

In the following, when we explore the laser power and linewidth, all these detunings are assumed to be zero. When calculating the pulling coefficients which describe the influence of these detunings on the laser frequency, we assume that they fluctuate around zero.

During the incoherent pumping process, the spontaneous decay of the electronic excited states and the loss of the photon from the cavity are also taken into account. The evolution of the atoms and cavity field density matrix $\hat{\rho}(t)$ is determined by the Born-Markov master equation

$$\begin{aligned}\frac{d}{dt}\hat{\rho} = {} & -i[\hat{H}_I, \hat{\rho}] + \kappa \mathscr{L}[\hat{a}]\hat{\rho} \\ & + \sum_{j=1}^{N} \left(\gamma_x \mathscr{L}\left[\hat{\sigma}_{xS}^{(j)}\right] + \gamma_P \mathscr{L}\left[\hat{\sigma}_{\mathrm{PS}}^{(j)}\right]\right)\hat{\rho} \\ & + \sum_{j=1}^{N} \left(\gamma_0 \mathscr{L}\left[\hat{\sigma}_{gx}^{(j)}\right] + \eta \mathscr{L}\left[\hat{\sigma}_{Sg}^{(j)}\right]\right)\hat{\rho}, \end{aligned} \tag{10}$$

with the Lindblad operator defined as

$$\mathscr{L}[\hat{\mathcal{O}}]\hat{\rho} \equiv \hat{\mathcal{O}}\hat{\rho}\hat{\mathcal{O}}^\dagger - \tfrac{1}{2}(\hat{\mathcal{O}}^\dagger\hat{\mathcal{O}}\hat{\rho} + \hat{\rho}\hat{\mathcal{O}}^\dagger\hat{\mathcal{O}}). \tag{11}$$

Here κ is the decay rate of the cavity photon; γ_0, γ_x, and γ_{P} are the spontaneous decay rates of the state $|x\rangle$ to $|g\rangle$, $|S\rangle$ to $|x\rangle$, and $|S\rangle$ to $|P\rangle$, respectively; and η characterizes the effective pumping rate from the ground state $|g\rangle$ to the state $|S\rangle$.

B. Calculation of laser power

In this work we solve the master equation (10) with the second-order mean-field approximation, where the correlations of three and more operators are ignored during the cumulant expansion [12,25,26], for example,

$$\langle\hat{A}\hat{B}\hat{C}\rangle \simeq \langle\hat{A}\rangle\langle\hat{B}\hat{C}\rangle + \langle\hat{B}\rangle\langle\hat{A}\hat{C}\rangle + \langle\hat{C}\rangle\langle\hat{A}\hat{B}\rangle - 2\langle\hat{A}\rangle\langle\hat{B}\rangle\langle\hat{C}\rangle. \tag{12}$$

Here we define the instantaneous and steady-state expectation values of operator $\hat{\mathcal{O}}$ as

$$\langle\hat{\mathcal{O}}\rangle \equiv \mathrm{Tr}[\hat{\mathcal{O}}\hat{\rho}(t)], \tag{13}$$

$$\langle\hat{\mathcal{O}}\rangle_s \equiv \mathrm{Tr}[\hat{\mathcal{O}}\hat{\rho}(\infty)]. \tag{14}$$

As all the coupling strengths are homogeneous with respect to the N atoms, the one- and two-operator expectation values are symmetric concerning the permutation of atoms. Therefore, we can write $\langle\hat{\sigma}_{\mu\nu}^{(j)}\rangle = \langle\hat{\sigma}_{\mu\nu}^{(1)}\rangle \equiv \langle\hat{\sigma}_{\mu\nu}\rangle$, $\langle\hat{\sigma}_{\mu\nu}^{(j)}\hat{a}\rangle = \langle\hat{\sigma}_{\mu\nu}^{(1)}\hat{a}\rangle \equiv \langle\hat{\sigma}_{\mu\nu}\hat{a}\rangle$, and $\langle\hat{\sigma}_{\mu\nu}^{(i)}\hat{\sigma}_{\mu'\nu'}^{(j)}\rangle_{i\neq j} = \langle\hat{\sigma}_{\mu\nu}^{(1)}\hat{\sigma}_{\mu'\nu'}^{(2)}\rangle \equiv \langle\hat{\sigma}_{\mu\nu}\hat{\sigma}_{\mu'\nu'}\rangle$ ($\mu, \nu = S, P, x, g$ and $i, j = 1, \ldots, N$).

Starting from the average photon number $\langle\hat{a}^\dagger\hat{a}\rangle$, we derive a series of dynamical equations of operator expectation values until they are closed, which are given in Appendix A. Then

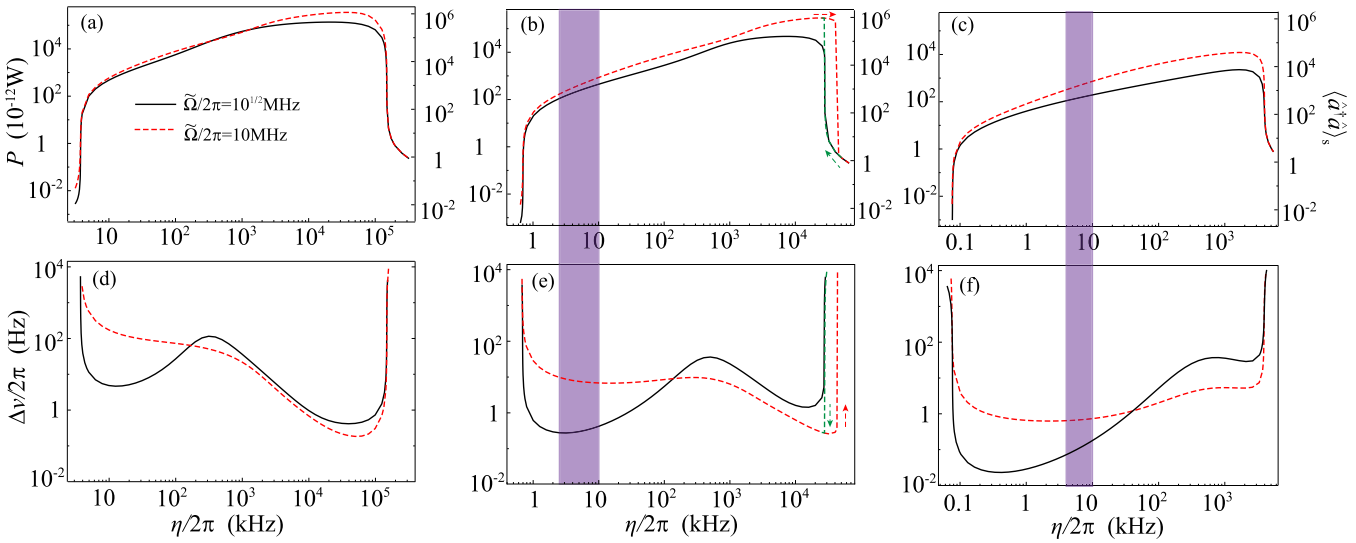

FIG. 2. Output power (average photon number) and linewidth of the superradiant laser as functions of pumping rate for the cases with (a) and (d) $\Omega_\alpha/\Omega_\beta = 1$, (b) and (e) $\Omega_\alpha/\Omega_\beta = 10^{1/2}$, and (c) and (f) $\Omega_\alpha/\Omega_\beta = 10$. The black solid and red dashed lines are plotted for $\tilde{\Omega} = 2\pi \times 10^{1/2}$ and $2\pi \times 10$ MHz, respectively. The regions satisfying $P \geqslant 10^{-10}$ W, $\Delta\nu \leqslant 2\pi \times 1$ Hz, and $\eta \leqslant 2\pi \times 10$ kHz can be found when $\Omega_\alpha/\Omega_\beta = 10^{1/2}$ and 10, as marked in purple. In (b) optical bistability appears when $\tilde{\Omega} = 2\pi \times 10$ MHz and the pumping strength is around the greater laser threshold ($\eta \sim 2\pi \times 20$ MHz), where the red (green) dashed line plots the laser power in the direction of increasing (decreasing) pumping rate.

we can obtain the steady-state photon number $\langle\hat{a}^\dagger\hat{a}\rangle_s$ and laser power $P \equiv \kappa\omega_c\langle\hat{a}^\dagger\hat{a}\rangle_s$ by numerically solving the above dynamical equations.

For each Raman intensity $\tilde{\Omega}$ and Raman ratio $\Omega_\alpha/\Omega_\beta$, the steady-state photon number $\langle\hat{a}^\dagger\hat{a}\rangle_s$ is a function of the pumping rate η. As shown in Fig. 2, in some regions of η, $\langle\hat{a}^\dagger\hat{a}\rangle_s$ is much larger than unity (e.g., 10^3–10^6). Outside these regions, $\langle\hat{a}^\dagger\hat{a}\rangle_s$ is only of the order of unity or even below. Moreover, at the border of these regions, $\langle\hat{a}^\dagger\hat{a}\rangle_s$ sharply increases or decreases with η. Apparently, the laser is generated in the regions with large $\langle\hat{a}^\dagger\hat{a}\rangle_s$. Hence, we define the value of η at the border of these regions as the laser threshold.[2]

C. Calculation of lasing frequency and linewidth

One cannot obtain the laser spectrum directly from the steady-state solutions of Eq. (10). Here we employ the filter-cavity method [17,25] to calculate the frequency and linewidth of the output laser numerically. Specifically, we assume that a low-dissipation filter cavity is weakly coupled with the laser cavity, which is described by the Hamiltonian

$$\hat{H}_f = \omega_b\hat{b}^\dagger\hat{b} + \zeta(\hat{b}^\dagger\hat{a} + \hat{a}^\dagger\hat{b}). \tag{15}$$

Here $\hat{b}$ is the photon annihilation operator of the filter cavity with angular frequency ω_b and ζ denotes its coupling strength with the lasing cavity. As both the dissipation rate of the filter cavity and its coupling with the laser mode are assumed to be much smaller than the Rabi frequencies and the dissipation rates of the lasing system, the filter cavity has a negligible influence on the lasing process. Meanwhile, the laser photon can enter into and dissipate from the filter cavity. Therefore, the spectrum of the steady-state photon number $\langle\hat{b}^\dagger\hat{b}\rangle_s$ versus the filter-cavity frequency ω_b will provide information about the laser frequency and linewidth of our scheme. As shown in Fig. 3, the spectrum of $\langle\hat{b}^\dagger\hat{b}\rangle_s$ has a single peak whose central frequency is just the lasing angular frequency ω^*. The full width at half maximum (FWHM) of this peak corresponds to the laser linewidth $\Delta\nu$ [17].

Before we present the numerical results, it is worth mentioning that the laser linewidth $\Delta\nu$ can also be obtained by the quantum regression theorem [12,27,28]. Though the quantum-regression method is not as efficient as the filter-cavity one for numerical calculation, it can give an approximate

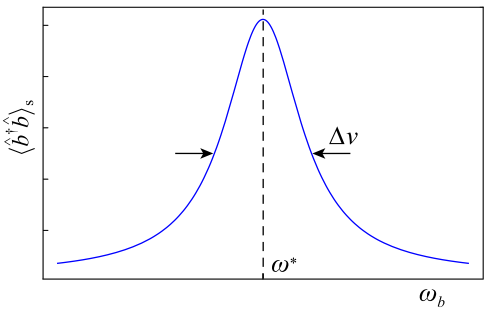

FIG. 3. Schematic diagram of the spectrum of filter cavity. The laser frequency and linewidth correspond to the central frequency and FWHM of this spectrum.

[2]Precisely speaking, the border of the regions with large $\langle\hat{a}^\dagger\hat{a}\rangle_s$ is not a single point on the η axis, but has finite width, as shown in Fig. 2. Here we just choose one point on the border to be the pumping threshold, and our result is not influenced by the chosen of this point.

expression of the laser linewidth in terms of $\langle\hat{\sigma}_{\mu\nu}\rangle_s$ ($\mu, \nu = S, P, x, g$) as

$$\Delta\nu = \left| \frac{\kappa + \frac{N\Omega_c^2}{F}\left[\eta\Omega_\alpha \mathrm{Im}\langle\hat{\sigma}_{Sx}\rangle_s + \Omega_\alpha\Omega_\beta \mathrm{Re}\langle\hat{\sigma}_{Px}\rangle_s - \left(\eta\Gamma + \Omega_\beta^2\right)\langle\hat{\sigma}_{xx} - \hat{\sigma}_{gg}\rangle_s\right]}{1 + \frac{\kappa}{F}\left[\eta\Gamma + (\gamma_0 + \eta)(\Gamma + \eta) + \Omega_\alpha^2 + \Omega_\beta^2\right] + \frac{N\Omega_c^2}{F}\left[\Omega_\alpha \mathrm{Im}\langle\hat{\sigma}_{Sx}\rangle_s - (\Gamma + \eta)\langle\hat{\sigma}_{xx} - \hat{\sigma}_{gg}\rangle_s\right]} \right|, \tag{16}$$

where we have defined $\Gamma = \gamma_x + \gamma_P + \eta$ and $F = \eta\Omega_\alpha^2 + (\gamma_0 + \eta)(\eta\Gamma + \Omega_\beta^2)$. The detailed derivation of Eq. (16) is given in Appendix B, which also shows that Eq. (16) coincides with the numerical result very well. We will discuss the effects of the dark-bright state coherence with the help of Eq. (16) in Sec. V.

IV. LASER PROPERTIES

In this section we consider an ensemble of cold alkaline-earth-metal ^{88}Sr atoms as the gain medium to illustrate the properties of the superradiant laser generated via our scheme. A laser using the same kind of atoms, but without the Raman beams, has been experimentally achieved in the superradiant crossover regime [15]. In our following second-order mean-field calculation, we adopt the parameters achievable in experiments, for instance, $N = 10^5$, $\kappa = 2\pi \times 150$ kHz, and $\Omega_c = 2\pi \times 21.2$ kHz. The spontaneous decay rates of the ^{88}Sr atom are $\gamma_x = 2\pi \times 2.6$ MHz, $\gamma_P = 2\pi \times 1.8$ MHz, and $\gamma_0 = 2\pi \times 7.5$ kHz [29].

A. Power and linewidth

We show the superradiant laser power P and the linewidth $\Delta\nu$ as functions of the pumping rate η in Fig. 2. The black solid (red dashed) lines represent the case with the Raman strength $\tilde{\Omega} = 2\pi \times 10^{1/2}$ MHz ($2\pi \times 10$ MHz) plotted for the Raman ratios $\Omega_\alpha/\Omega_\beta = 1$ [Figs. 2(a) and 2(d)], $\Omega_\alpha/\Omega_\beta = 10^{1/2}$ [Figs. 2(b) and 2(e)], and $\Omega_\alpha/\Omega_\beta = 10$ [Figs. 2(c) and 2(f)]. We see that the power P increases with the pumping rate η in the lasing regime, which is similar to other superradiant systems. However, in the pumping-linewidth curve, while only one minimum appears in the system without Raman beams [12,17], another local minimum point emerges in our scheme to the left of the former. Moreover, for proper Raman strengths and ratios, the new local minimum of linewidth becomes the global minimum with a pumping rate smaller than $2\pi \times 10$ kHz. This may inhibit the heating effect in the lasing process, which is helpful for the continuous output. Hence, the emergence of this new local minimum implies that our scheme may generate a narrow-linewidth ($2\pi \times 1$ Hz) laser with a considerable power (10^{-10} W) for practical use. For clarity, we mark the regions satisfying the conditions

$$P \geqslant 10^{-10}\ \mathrm{W}, \tag{17}$$

$$\Delta\nu \leqslant 2\pi \times 1\ \mathrm{Hz}, \tag{18}$$

$$\eta \leqslant 2\pi \times 10\ \mathrm{kHz} \tag{19}$$

in purple in Fig. 2.

We emphasize that the double-minimum behavior of linewidth is a characteristic resulting from the Raman-induced coherence, which is a significant difference of our superradiant lasing scheme from the previous works without Raman beams [12,16,17]. We leave the discussion of the underlying physics to Sec. V.

In Fig. 4 we provide more comprehensive information about our lasing scheme by two-dimensional plots of the laser

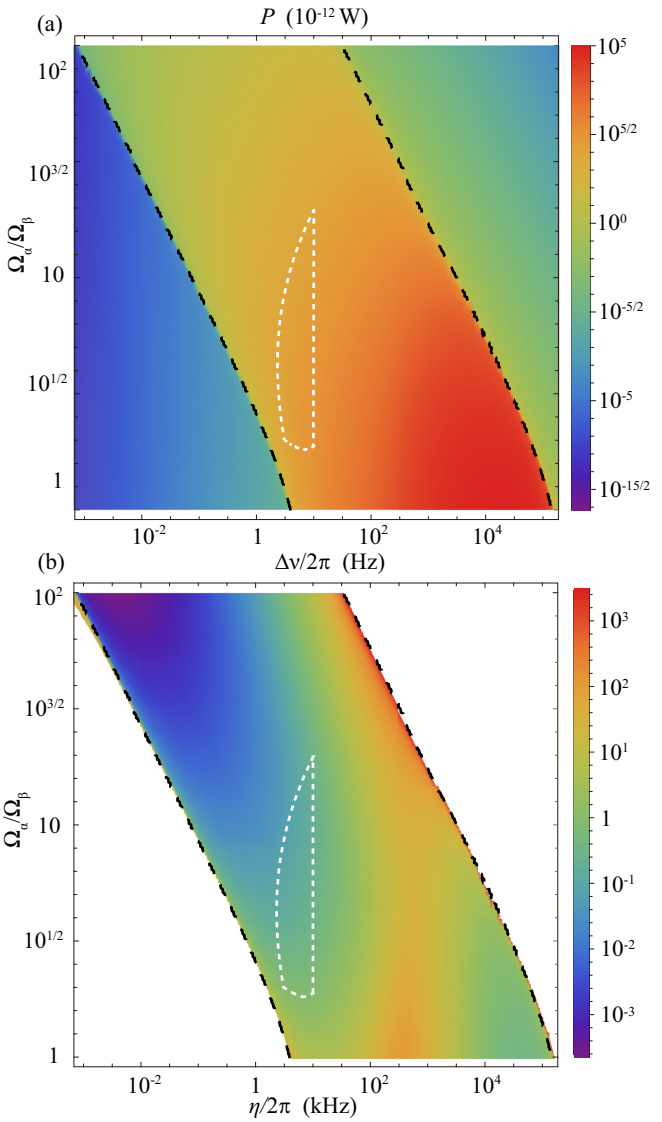

FIG. 4. Two-dimensional plots of (a) the power P and (b) the linewidth $\Delta\nu$ as functions of the pumping rate η and the Raman ratio $\Omega_\alpha/\Omega_\beta$. The thresholds of the laser scheme are illustrated by black dashed lines and the laser is generated in the regions in between. The area surrounded by the white dashed line represents the region satisfying $P \geqslant 10^{-10}$ W, $\Delta\nu \leqslant 2\pi \times 1$ Hz, and $\eta \leqslant 2\pi \times 10$ kHz. Here we set $\tilde{\Omega} = 2\pi \times 10^{1/2}$ MHz. In (b) we show only the linewidth in the lasing region.

power P and linewidth $\Delta\nu$ as functions of the pumping rate η and the Raman ratio $\Omega_\alpha/\Omega_\beta$. The Raman strength $\tilde{\Omega}$ is fixed at $2\pi \times 10^{1/2}$ MHz. The black dashed lines represent the threshold of our lasing scheme, and the area surrounded by the white dashed line shows the region satisfying Eqs. (17)–(19). In Fig. 4(b) we plot only the laser linewidth inside the lasing region.

Figure 4 shows that the Raman ratio $\Omega_\alpha/\Omega_\beta$ can be used to tune the laser power and linewidth. When increasing the Raman ratio, we find that both the laser power and linewidth, working around the left local minimum of linewidth, decrease continuously. Thus, there is competition between achieving considerable output power and keeping a small linewidth. In particular, when $\Omega_\alpha/\Omega_\beta$ is raised to the order of 10^2, we can realize the superradiant laser with a millihertz linewidth and 10^{-12}-W output power. This linewidth is at least six orders of magnitude smaller than the natural linewidth of the $^3P_1$ state of ^{88}Sr and comparable to that of the $^3P_0$ state of ^{87}Sr [12].

B. Lasing frequency and pulling coefficients

When the cavity mode is resonant with the atomic $^1S_0$ to $^3P_1$ transition ($\delta_c = 0$) and both of the Raman beams are resonant with the corresponding atomic transitions ($\delta_\alpha = \delta_\beta = 0$), numerical calculation shows that the central frequency ω^* of the output laser equals the atomic $^1S_0$ to $^3P_1$ transition frequency ω_0, i.e., $\omega^* = \omega_0$. Nevertheless, in realistic systems, fluctuations of the frequencies of the cavity mode and Raman beams (nonzero $\delta_{c,\alpha,\beta}$) will shift the lasing frequency from ω_0. The three pulling coefficients can describe the stability of the lasing frequency under these fluctuations,

$$c_p^{(i)} = \left|\frac{\partial\delta^*}{\partial\delta_i}\right|_{\delta_c=\delta_1=\delta_2=0} \quad (i = c, 1, 2), \tag{20}$$

where $\delta^* \equiv \omega^* - \omega_0$ is the fluctuation of the laser frequency and $\delta_1 \equiv \delta_\alpha + \delta_\beta$ ($\delta_2 \equiv \delta_\alpha - \delta_\beta$) is the one-photon (two-photon) detuning. According to the definition of δ_α and δ_β in Eqs. (8) and (9), the detunings δ_1 and δ_2 are determined by the summation and difference of the frequencies of the two Raman beams (i.e., $\omega_\alpha + \omega_\beta$ and $\omega_\alpha - \omega_\beta$), respectively.

In Fig. 5 we plot the pulling coefficients $c_p^{(c)}$, $c_p^{(1)}$, and $c_p^{(2)}$ as functions of the Raman ratio $\Omega_\alpha/\Omega_\beta$ and pumping rate η. Our results show that for $\eta \sim 2\pi \times 5$ kHz, we have $c_p^{(c)} \sim 10^{-2}$, $c_p^{(1)} \approx 0$, and $c_p^{(2)} \approx 1$. Therefore, in this region, the central frequency of the output laser is robust against the fluctuation of the cavity frequency and that of the frequency sum of the two Raman beams. However, the fluctuation of the frequency difference of the two Raman beams δ_2 results in an uncertainty of the central lasing frequency, which is approximately equal to δ_2. In the current experiments, via locking the two Raman beams with an optical comb or two modes of the same cavity [30], one can suppress $|\delta_2|$ to the level of hertz (or even lower). Therefore, the uncertainty of the central lasing frequency corresponding to δ_2 can approach the order of hertz as well.

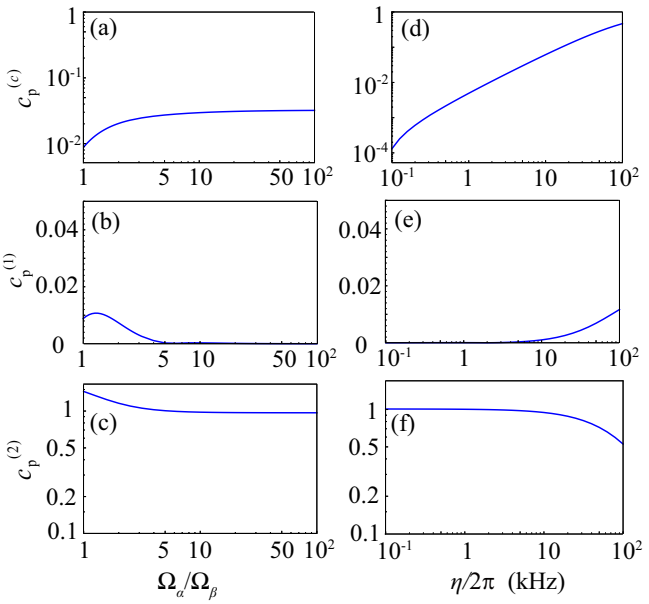

FIG. 5. Pulling coefficients $c_p^{(c)}$, $c_p^{(1)}$, and $c_p^{(2)}$ (a)–(c) as functions of the Raman ratio $\Omega_\alpha/\Omega_\beta$ with the pumping rate $\eta = 2\pi \times 5$ kHz and (d)–(f) as functions of the pumping rate η with the Raman ratio $\Omega_\alpha/\Omega_\beta = 10$. Here we set $\tilde{\Omega} = 2\pi \times 10^{1/2}$ MHz.

V. COHERENCE-INDUCED DOUBLE MINIMA OF THE LINEWIDTH

In the above sections we have demonstrated that the appearance of double minima in the pumping-linewidth curve is a crucial characteristic of our lasing scheme. Based on this fact, it is possible to realize a laser with a relatively small linewidth and high power at a low pumping rate (e.g., $\Delta\nu \leqslant 2\pi \times 1$ Hz and $P \geqslant 10^{-10}$ W at $\eta \leqslant 2\pi \times 10$ kHz). In this section we reveal that such a double-minimum feature stems from the Raman-induced coherence between the dark state $|D\rangle$ and the bright state $|B\rangle$. To this end, we illustrate the effect of this coherence from two aspects. First, we show that a simplified three-level model (TLM) cannot fully capture the features of the four-level lasing system; then, a rescaled coherence measure is defined for quantitative investigation.

A. Three-level models

In our system, as shown in Fig. 1(c), the atoms pumped to the state $|S\rangle$ can transit to both of the states $|D\rangle$ and $|B\rangle$ and then emit laser photons to the cavity mode. However, since the state $|S\rangle$ is coupled to $|B\rangle$ by the Raman beams, the atoms in state $|B\rangle$ can be repumped to $|S\rangle$. The atoms in state $|D\rangle$, in contrast, cannot directly transit back to $|S\rangle$ and have a 100% possibility to emit laser photons. The above facts indicate that it is the dark state rather than the bright one that dominates in the lasing process. Thus, a simplified TLM ignoring the state $|B\rangle$ may capture certain main properties, such as power and threshold, of our laser scheme.

In order to verify this thinking, we investigate a simplified TLM containing the atomic states $|g\rangle$, $|D\rangle$, and $|S\rangle$, which is referred to as a dark TLM and schematically shown in Fig. 6(a). Compared to the four-level model shown in Fig. 1(c), the dark TLM ignores the bright state $|B\rangle$ and the

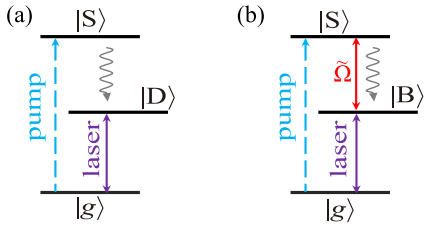

FIG. 6. Simplified three-level models used in Sec. V A. (a) The dark three-level model contains the ground state $|g\rangle$, the ${}^1S_0$ state $|S\rangle$, and the dark state $|D\rangle$. (b) The bright three-level model contains the bright state $|B\rangle$ instead of $|D\rangle$. In addition, an effective transition induced by the Raman beams couples the state $|B\rangle$ with $|S\rangle$.

spontaneous-decay-induced coupling between $|D\rangle$ and $|B\rangle$. As the dark state $|D\rangle$ is a superposition of the atomic states $|x\rangle$ and $|P\rangle$ [see Eq. (2)], the parameters used here are also superposed on those of the states $|x\rangle$ and $|P\rangle$. For instance, the spontaneous decay rates of state $|S\rangle$ to $|D\rangle$ and $|D\rangle$ to $|g\rangle$ are $(\Omega_\alpha^2\gamma_P + \Omega_\beta^2\gamma_x)/\tilde{\Omega}^2$ and $\Omega_\beta^2\gamma_0/\tilde{\Omega}^2$. The Rabi frequency of the coupling between the state $|D\rangle$ and the cavity mode is $\Omega_\beta\Omega_c/\tilde{\Omega}$.

We calculate the output power of the dark TLM with the second-order mean-field method and compare the result with that of the four-level scheme given in Sec. IV. As shown in Fig. 7, the laser power and threshold of the dark TLM are very close to that of the four-level model. Nevertheless, the laser linewidth of the dark TLM has only one minimum at about $\eta = 2\pi \times 10^4$ kHz, while another local minimum emerges in the four-level model at around $\eta = 2\pi \times 3$ kHz. Moreover,

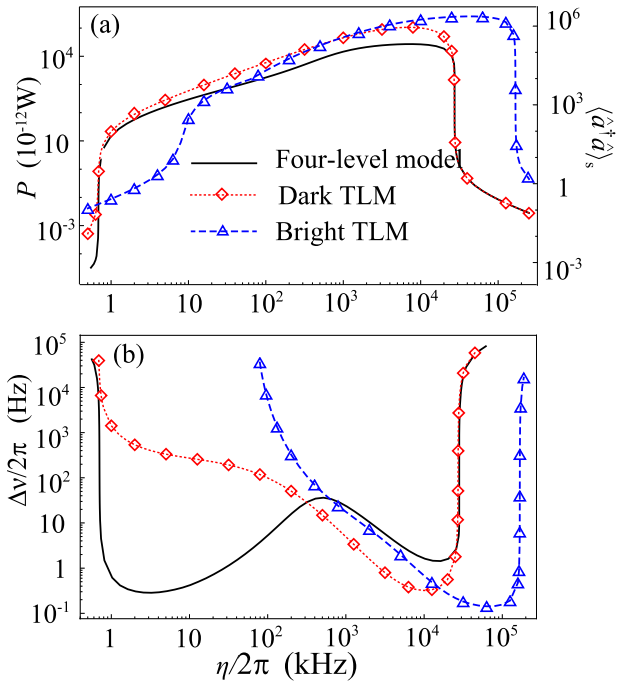

FIG. 7. Comparison of (a) the laser output power and (b) the linewidth of the four-level lasing model in Sec. II (black solid lines), the dark TLM (red dotted lines with diamonds), and the bright TLM (blue dashed lines with triangles). Here we set $\Omega_\alpha/\Omega_\beta = 10^{1/2}$ and $\tilde{\Omega} = 2\pi \times 10^{1/2}$ MHz.

near the new local minimum, the linewidth of the four-level model is of the subhertz level and three orders of magnitude smaller than that of the dark TLM. The above results yield that the dark lasing state alone cannot explain all the properties of the four-level model, especially the double-minimum behavior of the linewidth as a function of the pumping rate.

As a comparison, we also investigate a bright TLM, which contains the atomic states $|g\rangle$, $|B\rangle$, and $|S\rangle$, as shown in Fig. 6(b). Unlike the dark TLM, in the bright TLM, the $|B\rangle$ state coherently couples to the $|S\rangle$ state with an effective coupling strength $\tilde{\Omega}$ induced by the Raman beams. The other parameters are similar to those in the dark TLM. In Fig. 7, the blue dashed lines with triangles show the power and linewidth of the bright TLM, which are much different from those of the four-level model.

Clearly, neither the dark state nor the bright one alone is the reason for the double-minimum linewidth of the four-level model. The failure of these two TLMs suggests that the coherence between $|D\rangle$ and $|B\rangle$ may play a significant role in the double-minimum behavior.

B. Coherence between the dark and bright states

The steady-state expectation value $\langle\hat{\sigma}_{BD}\rangle_s \equiv \mathrm{Tr}[|B\rangle\langle D|\hat{\rho}(\infty)]$ naturally measures the coherence between the dark and bright states. When rewriting the linewidth equation (16) with the basis of the states $|D\rangle$ and $|B\rangle$, we can find that the term $\langle\hat{\sigma}_{BD}\rangle_s$ explicitly appears in the expression of $\Delta\nu$. However, the direct comparison of $\langle\hat{\sigma}_{BD}\rangle_s$ between different parameter cases is meaningless because the populations in the dark and bright states vary with η and $\Omega_{\alpha(\beta)}$. Therefore, we define a rescaled measure of coherence as

$$C_{BD} = \frac{|\langle\hat{\sigma}_{BD}\rangle_s|}{\langle\hat{\sigma}_{DD}\rangle_s + \langle\hat{\sigma}_{BB}\rangle_s}, \tag{21}$$

where $\langle\hat{\sigma}_{DD}\rangle_s$ and $\langle\hat{\sigma}_{BB}\rangle_s$ are the steady-state populations of the dark and bright states, respectively.

In Fig. 8 we plot the laser linewidth and the corresponding coherence measure C_{BD} with different values of $\tilde{\Omega}$ as a function of the pumping rate η. Here we choose the same value of $\Omega_\alpha/\Omega_\beta = 10^{1/2}$ as in Fig. 7. It can be seen from Fig. 8(a) that the double-minimum behavior of $\Delta\nu$ is more obvious for small Raman strength $\tilde{\Omega}$. When we increase the Raman strength $\tilde{\Omega}$ from $2\pi \times 10^{1/2}$ to $2\pi \times 10$ MHz, the left local minimum of the linewidth increases from below $2\pi \times 1$ Hz to $2\pi \times 10$ Hz. Further increasing the Raman strength to $2\pi \times 10^2$ MHz, we see that the double-minimum curve reduces to a single-minimum one which coincides with that of the dark TLM. Meanwhile, the rescaled coherence C_{BD} corresponding to the left local minimum of linewidth decreases from the order of 10^{-1} to 10^{-5} as $\tilde{\Omega}$ increases from $2\pi \times 10^{1/2}$ to $2\pi \times 10^2$ MHz [see Fig. 8(b)]. Such a correlation between a large C_{BD} and the double-minimum behavior of the linewidth confirms the importance of the coherence between the dark and bright states in our lasing scheme.

The coherence between the dark and bright states is also crucial in reducing the linewidth of ^{88}Sr superradiant lasing in the scheme discussed in Ref. [25]. Unlike our approach where the dark state is decoupled from the Raman lights, in Ref. [25] the dark state (the same as $|x\rangle$ in our work) corresponds to

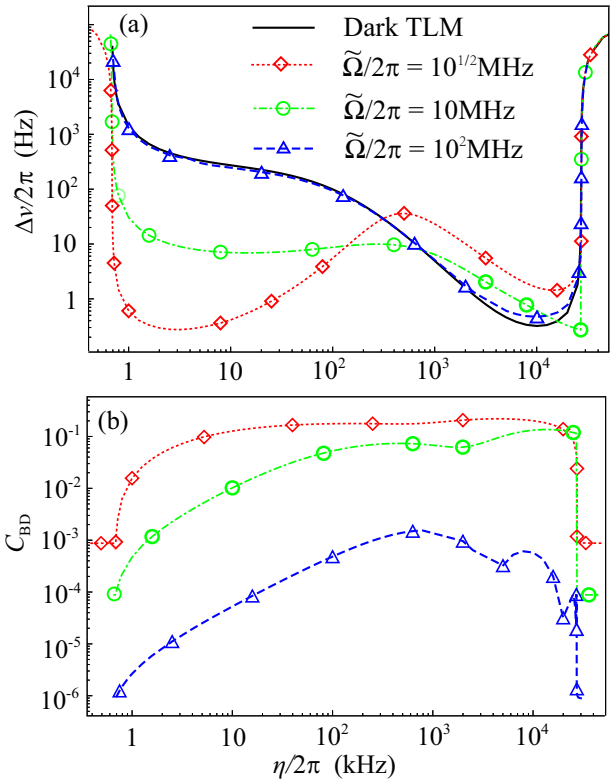

FIG. 8. (a) Linewidth $\Delta\nu$ and (b) rescaled coherence C_{BD} of the four-level lasing model introduced in Sec. II. The results are plotted for $\tilde{\Omega} = 2\pi \times 10^{1/2}$ MHz (red dotted line with diamonds), $\tilde{\Omega} = 2\pi \times 10$ MHz (green dash-dotted line with circles), and $2\pi \times 10^2$ MHz (blue dashed line with triangles). The linewidth of the dark TLM is also displayed with the black solid line for comparison. Here we have chosen the Raman ratio $\Omega_\alpha/\Omega_\beta = 10^{1/2}$.

a state that does not interact with the cavity mode, and the coherence between dark and bright states is induced by the presence of a magnetic field.

VI. CONCLUSION

In this work we have proposed a quantum-coherence-assisted superradiant laser scheme with bosonic alkaline-earth-metal atoms. The Raman beams play two critical roles here. First, they induce the steady-state coherence between the dark and bright states which produces a new local minimum in the pumping-linewidth curve with a small pumping rate. Thus our scheme can achieve a narrow-linewidth (less than approximately $2\pi \times 1$ Hz) and high-power (greater than approximately 10^{-10} W, approximately 10^3 photons in the steady state) output laser with a low pump (less than approximately $2\pi \times 10$ kHz). Second, as the Raman beams mix the long-lived $^3P_0$ state into the lasing state, the linewidth of our scheme is tunable with the Raman beams.

To illustrate the significance of the coherence between the dark and bright states in our scheme, we investigate two simplified three-level laser models which ignore the bright or dark state separately. A rescaled quantity is also introduced to measure the coherence between these two states. Calculations show a strong correlation between the double-minimum feature of linewidth and a large rescaled coherence measure. The lasing frequency is robust against the fluctuations of the cavity length and the one-photon detuning. Although a nonzero two-photon detuning will fluctuate the laser frequency with almost the same amount, this two-photon detuning can be well controlled by locking the two Raman beams to an optical comb or two modes of the same cavity. There are still some unresolved questions pertaining to the physical explanation of our lasing scheme. One may ask, for instance, why the three-level model (dark TLM) agrees with the four-level model for a very large Rabi strength $\tilde{\Omega}$.[3] Also, why does line narrowing occur at low pump strengths when the Raman ratio $\Omega_\alpha/\Omega_\beta$ is increased? The underlying physics, perhaps from the perspective of noise reduction, warrants further investigation.

Based on these achievements, our work greatly improves the output performance of the superradiant laser system with coherence induced by Raman transitions and may offer a firm foundation for its practical use in the future.

ACKNOWLEDGMENTS

G.D. thank Dr. Jin-Fu Chen for very helpful discussions. We thank the referees for their valuable suggestions. G.D. was supported by NSFC Grant No. 12205211. Y.Y. was supported by NSFC Grant No. 12175204. P.Z. was supported by National Key Research and Development Program of China Grant No. 2018YFA0306502 and NSAF Grant No. U1930201. D.X. was supported by NSFC Grant No. 12075025.

APPENDIX A: MEAN-FIELD DYNAMICAL EQUATIONS

Using the second-order mean-field theory described in the main text, a set of closed equations of motion for the expectation values of operators are obtained and listed as follows:

$$\frac{d}{dt}\langle\hat{a}^\dagger\hat{a}\rangle = -\kappa\langle\hat{a}^\dagger\hat{a}\rangle + i\frac{N\Omega_c}{2}(\langle\hat{\sigma}_{xg}\hat{a}\rangle - \text{H.c.}),$$

$$\frac{d}{dt}\langle\hat{\sigma}_{xg}\hat{a}\rangle = -\left[i\delta_c + \frac{1}{2}(\gamma_0 + \eta + \kappa)\right]\langle\hat{\sigma}_{xg}\hat{a}\rangle + i\frac{\Omega_\alpha}{2}\langle\hat{\sigma}_{Sg}\hat{a}\rangle - i\frac{\Omega_c}{2}[\langle\hat{\sigma}_{xx}\rangle + \langle\hat{a}^\dagger\hat{a}\rangle(\langle\hat{\sigma}_{xx}\rangle - \langle\hat{\sigma}_{gg}\rangle) + (N-1)\langle\hat{\sigma}_{xg}\hat{\sigma}_{gx}\rangle],$$

$$\frac{d}{dt}\langle\hat{\sigma}_{Pg}\hat{a}\rangle = \left[i(\delta_\alpha - \delta_\beta - \delta_c) - \frac{1}{2}(\eta + \kappa)\right]\langle\hat{\sigma}_{Pg}\hat{a}\rangle + i\frac{\Omega_\beta}{2}\langle\hat{\sigma}_{Sg}\hat{a}\rangle - i\frac{\Omega_c}{2}[\langle\hat{a}\hat{a}^\dagger\rangle\langle\hat{\sigma}_{Px}\rangle + (N-1)\langle\hat{\sigma}_{Pg}\hat{\sigma}_{gx}\rangle],$$

[3]One possible reason is that the large Raman coupling between $|S\rangle$ and $|B\rangle$ drives the atom from $|B\rangle$ to $|S\rangle$, which then decays partially to $|D\rangle$. Consequently, even though both the bright and dark states couple with the lasing mode, the population inversion mainly occurs between $|D\rangle$ and $|g\rangle$. Furthermore, $\tilde{\Omega}^2$, the coherence between $|B\rangle$ and $|D\rangle$ is substantially diminished (see Fig. 8). As a result, our lasing scheme behaves similarly to the dark TLM in the presence of a large Raman strength.

$$\frac{d}{dt}\langle\hat{\sigma}_{Sg}\hat{a}\rangle = \left[i(\delta_\alpha-\delta_c)-\frac{1}{2}(\Gamma+\kappa)\right]\langle\hat{\sigma}_{Sg}\hat{a}\rangle + i\frac{\Omega_\alpha}{2}\langle\hat{\sigma}_{xg}\hat{a}\rangle + i\frac{\Omega_\beta}{2}\langle\hat{\sigma}_{Pg}\hat{a}\rangle - i\frac{\Omega_c}{2}[\langle\hat{a}\hat{a}^\dagger\rangle\langle\hat{\sigma}_{Sx}\rangle + (N-1)\langle\hat{\sigma}_{Sg}\hat{\sigma}_{gx}\rangle],$$

$$\frac{d}{dt}\langle\hat{\sigma}_{xg}\hat{\sigma}_{gx}\rangle = -(\gamma_0+\eta)\langle\hat{\sigma}_{xg}\hat{\sigma}_{gx}\rangle + \left(i\frac{\Omega_\alpha}{2}\langle\hat{\sigma}_{Sg}\hat{\sigma}_{gx}\rangle + \text{H.c.}\right) + \left(i\frac{\Omega_c}{2}\langle\hat{\sigma}_{xg}\hat{a}\rangle + \text{H.c.}\right)(\langle\hat{\sigma}_{xx}\rangle - \langle\hat{\sigma}_{gg}\rangle),$$

$$\frac{d}{dt}\langle\hat{\sigma}_{xg}\hat{\sigma}_{gP}\rangle = \left[-i(\delta_\alpha-\delta_\beta)-\frac{1}{2}(\gamma_0+2\eta)\right]\langle\hat{\sigma}_{xg}\hat{\sigma}_{gP}\rangle + i\frac{\Omega_\alpha}{2}\langle\hat{\sigma}_{Sg}\hat{\sigma}_{gP}\rangle - i\frac{\Omega_\beta}{2}\langle\hat{\sigma}_{xg}\hat{\sigma}_{gS}\rangle + i\frac{\Omega_c}{2}[\langle\hat{\sigma}_{xg}\hat{a}\rangle\langle\hat{\sigma}_{xP}\rangle - \langle\hat{a}^\dagger\hat{\sigma}_{gP}\rangle(\langle\hat{\sigma}_{xx}\rangle - \langle\hat{\sigma}_{gg}\rangle)],$$

$$\begin{aligned}\frac{d}{dt}\langle\hat{\sigma}_{xg}\hat{\sigma}_{gS}\rangle = &\left[-i\delta_\alpha-\frac{1}{2}(\gamma_0+\Gamma+\eta)\right]\langle\hat{\sigma}_{xg}\hat{\sigma}_{gS}\rangle + i\frac{\Omega_\alpha}{2}(\langle\hat{\sigma}_{Sg}\hat{\sigma}_{gS}\rangle - \langle\hat{\sigma}_{xg}\hat{\sigma}_{gx}\rangle) - i\frac{\Omega_\beta}{2}\langle\hat{\sigma}_{xg}\hat{\sigma}_{gP}\rangle\\ &- i\frac{\Omega_c}{2}\langle\hat{a}^\dagger\hat{\sigma}_{gS}\rangle(\langle\hat{\sigma}_{xx}\rangle - \langle\hat{\sigma}_{gg}\rangle) + i\frac{\Omega_c}{2}\langle\hat{\sigma}_{xS}\rangle\langle\hat{\sigma}_{xg}\hat{a}\rangle,\end{aligned}$$

$$\frac{d}{dt}\langle\hat{\sigma}_{Pg}\hat{\sigma}_{gP}\rangle = -\eta\langle\hat{\sigma}_{Pg}\hat{\sigma}_{gP}\rangle + \left(i\frac{\Omega_c}{2}\langle\hat{\sigma}_{Pg}\hat{a}\rangle\langle\hat{\sigma}_{xP}\rangle - i\frac{\Omega_\beta}{2}\langle\hat{\sigma}_{Pg}\hat{\sigma}_{gS}\rangle + \text{H.c.}\right),$$

$$\frac{d}{dt}\langle\hat{\sigma}_{Pg}\hat{\sigma}_{gS}\rangle = \left[-i\delta_\beta-\frac{1}{2}(\Gamma+\eta)\right]\langle\hat{\sigma}_{Pg}\hat{\sigma}_{gS}\rangle - i\frac{\Omega_\alpha}{2}\langle\hat{\sigma}_{Pg}\hat{\sigma}_{gx}\rangle + i\frac{\Omega_\beta}{2}(\langle\hat{\sigma}_{Sg}\hat{\sigma}_{gS}\rangle - \langle\hat{\sigma}_{Pg}\hat{\sigma}_{gP}\rangle) + i\frac{\Omega_c}{2}(\langle\hat{\sigma}_{Pg}\hat{a}\rangle\langle\hat{\sigma}_{xS}\rangle - \langle\hat{\sigma}_{Px}\rangle\langle\hat{a}^\dagger\hat{\sigma}_{gS}\rangle),$$

$$\frac{d}{dt}\langle\hat{\sigma}_{Sg}\hat{\sigma}_{gS}\rangle = -\Gamma\langle\hat{\sigma}_{Sg}\hat{\sigma}_{gS}\rangle + \left(i\frac{\Omega_\alpha}{2}\langle\hat{\sigma}_{xg}\hat{\sigma}_{gS}\rangle + i\frac{\Omega_\beta}{2}\langle\hat{\sigma}_{Pg}\hat{\sigma}_{gS}\rangle + i\frac{\Omega_c}{2}\langle\hat{\sigma}_{Sg}\hat{a}\rangle\langle\hat{\sigma}_{xS}\rangle + \text{H.c.}\right),$$

$$\frac{d}{dt}\langle\hat{\sigma}_{xx}\rangle = -\gamma_0\langle\hat{\sigma}_{xx}\rangle + \gamma_x\langle\hat{\sigma}_{SS}\rangle + \left(-i\frac{\Omega_\alpha}{2}\langle\hat{\sigma}_{xS}\rangle + i\frac{\Omega_c}{2}\langle\hat{a}^\dagger\hat{\sigma}_{gx}\rangle + \text{H.c.}\right),$$

$$\frac{d}{dt}\langle\hat{\sigma}_{PP}\rangle = \gamma_P\langle\hat{\sigma}_{SS}\rangle - \left(i\frac{\Omega_\beta}{2}\langle\hat{\sigma}_{PS}\rangle + \text{H.c.}\right),$$

$$\frac{d}{dt}\langle\hat{\sigma}_{SS}\rangle = -(\gamma_x+\gamma_P)\langle\hat{\sigma}_{SS}\rangle + \eta\langle\hat{\sigma}_{gg}\rangle + \left(i\frac{\Omega_\alpha}{2}\langle\hat{\sigma}_{xS}\rangle + i\frac{\Omega_\beta}{2}\langle\hat{\sigma}_{PS}\rangle + \text{H.c.}\right),$$

$$\frac{d}{dt}\langle\hat{\sigma}_{xP}\rangle = \left[-i(\delta_\alpha-\delta_\beta)-\frac{1}{2}\gamma_0\right]\langle\hat{\sigma}_{xP}\rangle + i\frac{\Omega_\alpha}{2}\langle\hat{\sigma}_{SP}\rangle - i\frac{\Omega_\beta}{2}\langle\hat{\sigma}_{xS}\rangle + i\frac{\Omega_c}{2}\langle\hat{a}^\dagger\hat{\sigma}_{gP}\rangle,$$

$$\frac{d}{dt}\langle\hat{\sigma}_{xS}\rangle = \left[-i\delta_\alpha-\frac{1}{2}(\gamma_0+\gamma_x+\gamma_P)\right]\langle\hat{\sigma}_{xS}\rangle + i\frac{\Omega_\alpha}{2}(\langle\hat{\sigma}_{SS}\rangle - \langle\hat{\sigma}_{xx}\rangle) - i\frac{\Omega_\beta}{2}\langle\hat{\sigma}_{xP}\rangle + i\frac{\Omega_c}{2}\langle\hat{a}^\dagger\hat{\sigma}_{gS}\rangle,$$

$$\frac{d}{dt}\langle\hat{\sigma}_{PS}\rangle = \left[-i\delta_\beta-\frac{1}{2}(\gamma_x+\gamma_P)\right]\langle\hat{\sigma}_{PS}\rangle - i\frac{\Omega_\alpha}{2}\langle\hat{\sigma}_{Px}\rangle + i\frac{\Omega_\beta}{2}(\langle\hat{\sigma}_{SS}\rangle - \langle\hat{\sigma}_{PP}\rangle).$$

Here we have used the relation $\langle\hat{\sigma}_{gg}\rangle + \langle\hat{\sigma}_{xx}\rangle + \langle\hat{\sigma}_{SS}\rangle + \langle\hat{\sigma}_{PP}\rangle = 1$.

As the coherence between the bright and dark states plays a significant role in our lasing scheme, here we rewrite the dynamical equation of the expectation value of the coherence term $\hat{\sigma}_{BD}$ in the basis of the bright and dark states

$$\begin{aligned}\frac{d}{dt}\langle\hat{\sigma}_{BD}\rangle = &-\left(i\delta_2\frac{\Omega_\alpha^2-\Omega_\beta^2}{\tilde{\Omega}^2}+\frac{\gamma_0}{2}\right)\langle\hat{\sigma}_{BD}\rangle + \frac{\Omega_\alpha\Omega_\beta}{\tilde{\Omega}^2}\left(i\delta_2-\frac{\gamma_0}{2}\right)\langle\hat{\sigma}_{BB}\rangle - \frac{\Omega_\alpha\Omega_\beta}{\tilde{\Omega}^2}\left(i\delta_2+\frac{\gamma_0}{2}\right)\langle\hat{\sigma}_{DD}\rangle\\ &+ (\gamma_x-\gamma_P)\frac{\Omega_\alpha\Omega_\beta}{\tilde{\Omega}^2}\langle\hat{\sigma}_{SS}\rangle - i\frac{\Omega_\beta}{\tilde{\Omega}}\frac{\Omega_c}{2}\langle\hat{\sigma}_{Bg}\hat{a}\rangle + i\frac{\Omega_c}{2}\frac{\Omega_\alpha}{\tilde{\Omega}}\langle\hat{a}^\dagger\hat{\sigma}_{gD}\rangle + i\frac{\tilde{\Omega}}{2}\langle\hat{\sigma}_{SD}\rangle. \qquad \text{(A1)}\end{aligned}$$

Hence, for the case of zero two-photon detuning, as discussed in the main text, the coupling between the dark and bright states mainly arises from the terms in the second line of Eq. (A1). These terms include the spontaneous decay of $|S\rangle$, the coupling between the cavity mode and the $|B\rangle$-$|g\rangle$ and $|D\rangle$-$|g\rangle$ transitions, and the Raman coupling. The corresponding strength is related to $(\gamma_x-\gamma_P)\Omega_\alpha\Omega_\beta/\tilde{\Omega}^2$, $\Omega_c\Omega_\beta/2\tilde{\Omega}$, $\Omega_c\Omega_\alpha/2\tilde{\Omega}$, and $\tilde{\Omega}/2$, respectively.

APPENDIX B: LINEWIDTH OBTAINED BY THE QUANTUM REGRESSION THEOREM

In this Appendix we show how to obtain the analytical expression of the linewidth via the quantum regression theorem.

1. Dynamical equations of the correlation functions

The laser linewidth $\Delta\nu$ can be read from the FWHM of the laser power spectrum $S(\omega)$, which is related to the two-time correlation function of the laser according to the Wiener-Khinchin theorem [31–33], i.e.,

$$S(\omega) = 2\int_0^\infty dt\,\text{Re}[\langle\hat{a}^\dagger(t)\hat{a}(0)\rangle_s e^{-i(\omega-\omega_0)t}]. \qquad \text{(B1)}$$

The two-time correlation function can be found using the quantum regression theorem, which reads

$$\frac{d}{dt}\langle\hat{a}^\dagger(t)\hat{a}(0)\rangle_s = \left(i\delta_c-\frac{\kappa}{2}\right)\langle\hat{a}^\dagger(t)\hat{a}(0)\rangle_s + \frac{iN\Omega_c}{2}\langle\hat{\sigma}_{xg}(t)\hat{a}(0)\rangle_s. \qquad \text{(B2)}$$

This equation contains another correlation function $\langle\hat{\sigma}_{xg}(t)\hat{a}(0)\rangle_s$. Thus, we continuously derive a set of equations of motion until they are closed under the second-order mean-field approximation as

$$\frac{d}{dt}A(t) = \mathbb{B}\cdot A(t), \tag{B3}$$

where

$$A(t) = [\langle\hat{a}^\dagger(t)\hat{a}(0)\rangle_s, \langle\hat{\sigma}_{xg}(t)\hat{a}(0)\rangle_s, \langle\hat{\sigma}_{Pg}(t)\hat{a}(0)\rangle_s, \langle\hat{\sigma}_{Sg}(t)\hat{a}(0)\rangle_s]^{\mathrm{T}} \tag{B4}$$

and

$$\mathbb{B} = -\frac{1}{2}\begin{pmatrix} -2i\delta_c+\kappa & -iN\Omega_c & 0 & 0 \\ i\Omega_c\langle\hat{\sigma}_{xx}-\hat{\sigma}_{gg}\rangle_s & \gamma_0+\eta & 0 & -i\Omega_\alpha \\ i\Omega_c\langle\hat{\sigma}_{Px}\rangle_s & 0 & -2i\delta_2+\eta & -i\Omega_\beta \\ i\Omega_c\langle\hat{\sigma}_{Sx}\rangle_s & -i\Omega_\alpha & -i\Omega_\beta & -2i\delta_\alpha+\Gamma \end{pmatrix}. \tag{B5}$$

The initial condition of Eq. (B3) is the steady-state solutions of the corresponding operators given in Appendix A.

2. Analytical solutions of the dynamical equations

As the matrix $\mathbb{B}$ is not Hermitian, its eigenvalues are not real, and the corresponding eigenvectors are not orthogonal. Before solving the dynamical equations (B3), we need to introduce the left and right eigenvectors of $\mathbb{B}$, which are defined as

$$\mathbb{B}|i\rangle = \lambda_i|i\rangle, \tag{B6}$$

$$\langle\tilde{i}|\mathbb{B} = \lambda_i\langle\tilde{i}|. \tag{B7}$$

In these equations λ_i $(i = 1, 2, 3, 4)$ is the ith eigenvalue of $\mathbb{B}$, and $\langle\tilde{i}|$ and $|i\rangle$ are the left and right eigenvectors of $\mathbb{B}$, respectively, which satisfy the relation $\langle\tilde{i}|j\rangle = \delta_{i,j}$ for $i, j = 1, 2, 3, 4$. Then the unit operator in this space becomes $I = \sum_i |i\rangle\langle\tilde{i}|$.

Next we perform the Laplace transformation to Eq. (B3) and obtain

$$\bar{A}(p) = \frac{1}{p-\mathbb{B}}A(0), \tag{B8}$$

where $\bar{A}(p)$ is the Laplace transform of $A(t)$. Inserting the operator $I = \sum_i |i\rangle\langle\tilde{i}|$ into Eq. (B8), we have

$$\bar{A}(p) = \sum_i \frac{1}{p-\lambda_i}|i\rangle\langle\tilde{i}|A(0). \tag{B9}$$

After applying the inverse Laplace transformation, we find the $A(t)$ as

$$A(t) = \sum_i e^{\lambda_i t}|i\rangle\langle\tilde{i}|A(0). \tag{B10}$$

Equation (B10) indicates that the two-time correlation function $\langle\hat{a}^\dagger(t)\hat{a}(0)\rangle_s$ is a superposition of the functions $e^{\lambda_i t}$ $(i = 1, 2, 3, 4)$. As the spectrum function $S(\omega)$ is the Fourier transform of the correlation function $\langle\hat{a}^\dagger(t)\hat{a}(0)\rangle_s$ [see Eq. (B1)], it is superposed by four Lorentzian line shapes whose central frequencies and linewidths are $\omega_0 + \mathrm{Im}(\lambda_i)$ and $2|\mathrm{Re}(\lambda_i)|$ $(i = 1, 2, 3, 4)$, respectively.

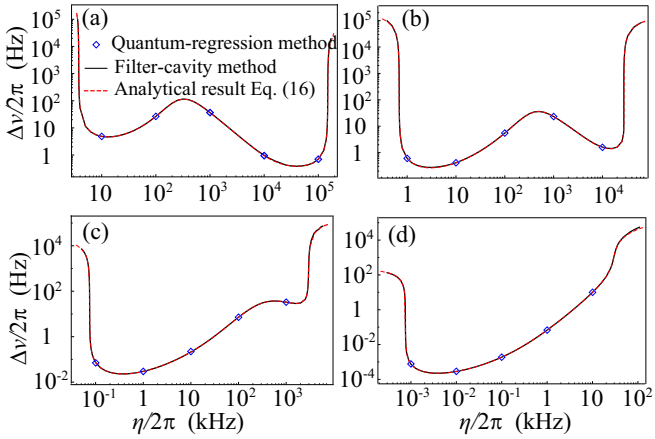

FIG. 9. Laser linewidth obtained by the quantum regression method (blue diamonds), the filter-cavity method (black solid lines), and the approximated analytical expression (16) (red dashed lines) for (a) $\Omega_\alpha/\Omega_\beta = 1$, (b) $\Omega_\alpha/\Omega_\beta = 10^{1/2}$, (c) $\Omega_\alpha/\Omega_\beta = 10$, and (d) $\Omega_\alpha/\Omega_\beta = 10^2$.

3. Approximate analytical expression of the linewidth

According to the numerical calculation, under the resonant condition that $\delta_c = \delta_\alpha = \delta_\beta = 0$, the central frequency ω^* of the output laser equals the atomic $^1S_0$ to $^3P_1$ transition frequency ω_0. This fact indicates that, among the four Lorentzian line shapes, the one corresponding to the eigenvalue with a zero imaginary part and a small real part contributes most significantly to the laser spectrum.

Therefore, we try to find the eigenvalue $\lambda_{\min}$ of the matrix $\mathbb{B}$ which has a zero imaginary part and a small real part. By solving the eigenfunction of $\mathbb{B}$ to the first order, we obtain an approximated expression

$$\lambda_{\min} \simeq \frac{iA_1 + A_2}{2B_1}, \tag{B11}$$

where A_1, A_2, and B_1 are real numbers and

$$\begin{aligned} B_1 \simeq{}& N\Omega_c^2[\Omega_\alpha \mathrm{Im}\langle\hat{\sigma}_{Sx}\rangle_s - (\Gamma+\eta)\langle\hat{\sigma}_{xx}-\hat{\sigma}_{gg}\rangle_s] \\ &+ \kappa[\eta\Gamma + (\gamma_0+\eta)(\Gamma+\eta)] + \gamma_0\Omega_\beta^2 \\ &+ (\eta+\kappa)\big(\Omega_\alpha^2+\Omega_\beta^2\big) + \eta\Gamma(\gamma_0+\eta), \\ A_1 \simeq{}& N\Omega_c^2\Omega_\alpha[\Omega_\beta \mathrm{Im}\langle\hat{\sigma}_{Px}\rangle_s - \eta\mathrm{Re}\langle\hat{\sigma}_{Sx}\rangle_s], \\ A_2 \simeq{}& \kappa\big[(\gamma_0+\eta)\Omega_\beta^2 + \eta\Omega_\alpha^2 + \eta\Gamma(\gamma_0+\eta)\big] \\ &- N\Omega_c^2\big(\eta\Gamma+\Omega_\beta^2\big)\langle\hat{\sigma}_{xx}-\hat{\sigma}_{gg}\rangle_s \\ &+ N\Omega_c^2\Omega_\alpha[\Omega_\beta \mathrm{Re}\langle\hat{\sigma}_{Px}\rangle_s + \eta\mathrm{Im}\langle\hat{\sigma}_{Sx}\rangle_s]. \end{aligned}$$

In the steady state, we numerically find that $\mathrm{Re}\langle\hat{\sigma}_{Sx}\rangle_s = \mathrm{Im}\langle\hat{\sigma}_{Px}\rangle_s = 0$, which verifies that the imaginary part of $\lambda_{\min}$ is zero. As the laser linewidth depends on the real part of $\lambda_{\min}$, we finally obtain the approximate analytical expression of the linewidth as

$$\Delta\nu = 2|\mathrm{Re}(\lambda_{\min})| = |A_2/B_1|, \tag{B12}$$

the explicit expression of which is given in Eq. (16).

We show the analytical expression (16) with the red dashed lines in Fig. 9. The numerical results using the quantum regression method and the filter-cavity method are also

presented with the blue diamonds and the black solid lines, respectively. The curves of the three methods coincide with each other very well and thus demonstrate the validity of our analytical expression.

[1] A. Abramovici, W. E. Althouse, R. W. P. Drever, Y. Gursel, S. Kawamura, F. J. Raab, D. Shoemaker, L. Sievers, R. E. Spero, K. S. Thorne, R. E. Vogt, R. Weiss, S. E. Whitcomb, and M. E. Zucker, Science **256**, 325 (1992).

[2] T. M. Fortier, N. Ashby, J. C. Bergquist, M. J. Delaney, S. A. Diddams, T. P. Heavner, L. Hollberg, W. M. Itano, S. R. Jefferts, K. Kim, F. Levi, L. Lorini, W. H. Oskay, T. E. Parker, J. Shirley, and J. E. Stalnaker, Phys. Rev. Lett. **98**, 070801 (2007).

[3] P. W. Graham, J. M. Hogan, M. A. Kasevich, and S. Rajendran, Phys. Rev. Lett. **110**, 171102 (2013).

[4] G. M. Harry, H. Armandula, E. Black, D. R. M. Crooks, G. Cagnoli, J. Hough, P. Murray, S. Reid, S. Rowan, P. Sneddon, M. M. Fejer, R. Route, and S. D. Penn, Appl. Opt. **45**, 1569 (2006).

[5] G. Rosi, F. Sorrentino, L. Cacciapuoti, M. Prevedelli, and G. M. Tino, Nature (London) **510**, 518 (2014).

[6] K. Numata, A. Kemery, and J. Camp, Phys. Rev. Lett. **93**, 250602 (2004).

[7] M. Notcutt, L.-S. Ma, J. Ye, and J. L. Hall, Opt. Lett. **30**, 1815 (2005).

[8] M. Notcutt, L.-S. Ma, A. D. Ludlow, S. M. Foreman, J. Ye, and J. L. Hall, Phys. Rev. A **73**, 031804(R) (2006).

[9] T. Kessler, C. Hagemann, C. Grebing, T. Legero, U. Sterr, F. Riehle, M. J. Martin, L. Chen, and J. Ye, Nat. Photon. **6**, 687 (2012).

[10] G. D. Cole, W. Zhang, M. J. Martin, J. Ye, and M. Aspelmeyer, Nat. Photon. **7**, 644 (2013).

[11] J. Chen, Chin. Sci. Bull. **54**, 348 (2009).

[12] D. Meiser, J. Ye, D. R. Carlson, and M. J. Holland, Phys. Rev. Lett. **102**, 163601 (2009).

[13] J. G. Bohnet, Z. Chen, J. M. Weiner, D. Meiser, M. J. Holland, and J. K. Thompson, Nature (London) **484**, 78 (2012).

[14] M. A. Norcia, M. N. Winchester, J. R. K. Cline, and J. K. Thompson, Sci. Adv. **2**, e1601231 (2016).

[15] M. A. Norcia and J. K. Thompson, Phys. Rev. X **6**, 011025 (2016).

[16] D. A. Tieri, M. Xu, D. Meiser, J. Cooper, and M. J. Holland, arXiv:1702.04830.

[17] K. Debnath, Y. Zhang, and K. Mølmer, Phys. Rev. A **98**, 063837 (2018).

[18] M. A. Norcia, R. J. Lewis-Swan, J. R. K. Cline, B. Zhu, A. M. Rey, and J. K. Thompson, Science **361**, 259 (2018).

[19] D. Meiser and M. J. Holland, Phys. Rev. A **81**, 033847 (2010).

[20] H. Liu, S. B. Jäger, X. Yu, S. Touzard, A. Shankar, M. J. Holland, and T. L. Nicholson, Phys. Rev. Lett. **125**, 253602 (2020).

[21] A. Shankar, J. T. Reilly, S. B. Jäger, and M. J. Holland, Phys. Rev. Lett. **127**, 073603 (2021).

[22] G. Dong, D. Xu, and P. Zhang, Phys. Rev. A **102**, 033717 (2020).

[23] M. N. Winchester, M. A. Norcia, J. R. K. Cline, and J. K. Thompson, Phys. Rev. Lett. **118**, 263601 (2017).

[24] R. Santra, K. V. Christ, and C. H. Greene, Phys. Rev. A **69**, 042510 (2004).

[25] Y. Zhang, C. Shan, and K. Mølmer, Phys. Rev. Lett. **126**, 123602 (2021).

[26] R. Kubo, J. Phys. Soc. Jpn. **17**, 1100 (1962).

[27] M. Lax, Phys. Rev. **129**, 2342 (1963).

[28] H.-P. Breuer and F. Petruccione, *The Theory of Open Quantum System* (Oxford University Press, Oxford, 2002).

[29] I. Courtillot, A. Quessada-Vial, A. Brusch, D. Kolker, G. D. Rovera, and P. Lemonde, Eur. Phys. J. D **33**, 161 (2005).

[30] T. Fortier and E. Baumann, Commun. Phys. **2**, 153 (2019).

[31] N. Wiener, Acta Math. **55**, 117 (1930).

[32] A. Khintchine, Math. Ann. **109**, 604 (1934).

[33] K. Huang, *Introduction to Statistical Physics* (Chapman and Hall/CRC, Boca Raton, 2009).